

Denitsa Milanova  
Robert D. Chambers  
Supreet S. Bahga  
Juan G. Santiago

Mechanical Engineering  
Department, Stanford University,  
CA, USA

Received April 7, 2011  
Revised August 3, 2011  
Accepted August 5, 2011

## Research Article

# Electrophoretic mobility measurements of fluorescent dyes using on-chip capillary electrophoresis

We present an experimental study of the effect of pH, ionic strength, and concentrations of the electroosmotic flow (EOF)-suppressing polymer polyvinylpyrrolidone (PVP) on the electrophoretic mobilities of commonly used fluorescent dyes (fluorescein, Rhodamine 6G, and Alexa Fluor 488). We performed on-chip capillary zone electrophoresis experiments to directly quantify the effective electrophoretic mobility. We use Rhodamine B as a fluorescent neutral marker (to quantify EOF) and CCD detection. We also report relevant acid dissociation constants and analyte diffusivities based on our absolute estimate (as per Nernst–Einstein diffusion). We perform well-controlled experiments in a pH range of 3–11 and ionic strengths ranging from 30 to 90 mM. We account for the influence of ionic strength on the electrophoretic transport of sample analytes through the Onsager and Fuoss theory extended for finite radii ions to obtain the absolute mobility of the fluorophores. Lastly, we briefly explore the effect of PVP on adsorption–desorption dynamics of all three analytes, with particular attention to cationic R6G.

### Keywords:

Absolute mobility / Alexa Fluor 488 / Electrophoretic mobility / Fluorescein / Rhodamine 6G  
DOI 10.1002/elps.201100210



## 1 Introduction

Fluorescent dyes are used in a wide range of applications including fluorescent probes [1]; fluorescent labels of nucleosides, nucleotides, and nucleic acids [2]; biomolecule characterization [3]; and pH indicators [4]. Most relevant here, they are frequently used as markers or labels in a wide variety of electrophoresis techniques including isoelectric focusing (IEF) [5, 6], capillary zone electrophoresis (CZE) [7, 8] and isotachopheresis (ITP) [9, 10]. The latter techniques rely on electromigration, so accurate characterization of ion electrophoretic mobility is essential. Given ionization state information, the electrophoretic mobility of an ion can also be used to estimate diffusivity; for example, via the well-known Nernst–Einstein relation [11]. Effective

(observable) electrophoretic mobility depends on pH and ionic strength (See [12, 13] for a description of effective versus fully ionized versus absolute mobility and their relations to ionic strength and pH.) and so systematic variation of these parameters is also important.

A straightforward approach to measure the electrophoretic mobility of chemical species is by CZE [14–19]. Effective electrophoretic mobility, the observable electrophoretic mobility of a dye, is measured by noting the time taken by an analyte peak to reach the detector (and correcting for electroosmotic flow, EOF). Capillary CE measurements of mobility are relatively simple (e.g. using a single, homogeneous buffer chemistry) and robust to trace impurities. One challenge of applying CZE is quantifying low magnitude mobilities, which can take overly long to reach a detector (yielding low signal-to-noise ratio). The latter has been addressed by, for example, using pressure injection of the analyte and the use of a neutral marker [20].

ITP offers an alternate method of quantifying mobilities [21–24]. ITP methods use a known leading electrolyte chemistry and focuses sample species into plateau mode (maximum, locally uniform concentration of the analyte) [21, 22] where purified analyte concentration (and zone order) can be related to analyte effective mobility. ITP is attractive as it can easily identify and quantify the mobility of multiple samples simultaneously, allows for low analyte

**Correspondence:** Professor Juan G. Santiago, Building 530, Room 225, Stanford University, 440 Escondido Mall, Stanford, CA 94305-3030, USA  
**E-mail:** juan.santiago@stanford.edu  
**Fax:** +1-650-723-7657

**Abbreviations:** AF488, Alexa Fluor 488; FCS, fluorescence correlation spectroscopy; FL, fluorescein; PVS, polyvinyl sulfate; RB, rhodamine B; R6G, rhodamine 6G

concentrations (order of nmol), and can be robust to trace impurities [25, 26]. Hirokawa et al. [21, 22] and Pospichal et al. [23, 24] used ITP to quantify the absolute mobilities (mobility of chemical species when it is fully ionized under infinite dilution) and acid dissociation constant ( $pK_a$ ) for a number of compounds with sufficiently high accuracy and good reproducibility.

In the current effort to directly quantify the mobility of fluorophores, we chose CZE over ITP as CZE offers more direct control of pH throughout the system. In CZE, pH and ionic strength in the separation channel are uniform and determined directly by the background buffer chemistry, which can be quantified *ex situ*. Furthermore, CZE is easily compatible with systems with unsuppressed EOF, as CZE avoids non-uniform electric fields and non-uniform electroosmotic mobilities which can give rise to significant analyte zone dispersion [27, 28].

In the current paper, we present measurements of absolute and effective electrophoretic mobilities, and diffusivities of three commonly used, namely fluorescent species fluorescein (anionic sodium fluorescein, FL), Rhodamine 6G (cationic Rhodamine 6G chloride, R6G), and Alexa Fluor 488 (anionic Alexa Fluor 488 succinimidyl ester, AF488). There are several references reporting mobility values of FL [29–31], but surprisingly we know of no quantitative study of the absolute mobility and  $pK_a$  of R6G or AF488. We also explore the effect of polyvinylpyrrolidone (PVP) concentration on the mobility of these three dyes. PVP is used commonly as dynamic wall coating for suppressing EOF [32, 33] and yet we know of no such studies. We use on-chip CZE and CCD camera detection to quantify effective mobilities in a pH range of 3–11 and ionic strengths ranging from 30 to 90 mM. We use Rhodamine B (RB) as a neutral fluorescent tracer reference and to quantify EOF mobilities. We analyze these data to report values of absolute mobility [34] for FL, R6G, and AF488. Where relevant, we experimentally quantify  $pK_a$  for effective mobility estimates. We account for and correct for the influence of ionic strength on all mobility measurements. This approach leverages the speed, low sample use, and relatively low cost of on-chip electrophoresis experiments. Our overall intent is to present a case study of how on-chip systems can be used to obtain accurate, highly reproducible mobility measurements with minimal sample use; while also providing unique data for AF488 and R6G mobility in free solution and the effect of PVP on the mobilities of FL, AF488, and (most interestingly) R6G. When applicable, we highlight the methods and issues relevant to leveraging on-chip systems to quantify ion mobilities.

## 2 Theory

We here review relevant electrophoretic mobility theory, which we used to interpret and standardize our measurements. The ‘actual mobility’  $\mu_i$  of an ion is defined as the electrophoretic mobility of the molecule in its fully ionized

state at a particular integer valence and at a particular finite ionic strength [34]. The degree of disassociation and the effective mobility of weak electrolytes depend on the pH of solution [12, 34]. Electrophoretic mobility of a partially ionized species in a solution is termed ‘effective mobility’ [12, 34]. CZE experiments are typically performed in well-buffered solutions of known pH where weak electrolytes are often partially dissociated. Therefore, effective mobility is typically the empirically relevant, observable quantity. Effective mobility  $\mu_{i,\text{eff}}$  is related to the degree of dissociation  $g_{i,z}$  and actual mobility  $\mu_{i,z}$  of species  $i$  and valence state  $z$  by [12]

$$\mu_{i,\text{eff}} = \sum_z \mu_{i,z} g_{i,z} \quad (1)$$

For example, the degree of dissociation and the effective mobility of a weak monovalent acid depend on the pH and acid dissociation constant  $pK_{-1}$  as

$$\mu_{i,\text{eff}} = \mu_{i,-1} g_{i,-1} = \mu_{i,-1} \frac{1}{1 + 10^{pK_{-1} - \text{pH}}} \quad (2)$$

The effective mobility of a divalent acid depends on the dissociation level of the  $-1$  and  $-2$  valence states as

$$\begin{aligned} \mu_{i,\text{eff}} &= \mu_{i,-1} g_{i,-1} + \mu_{i,-2} g_{i,-2} \\ &= \frac{\mu_{i,-1} + \mu_{i,-2} 10^{\text{pH} - pK_{-2}}}{1 + 10^{pK_{-1} - \text{pH}} + 10^{\text{pH} - pK_{-2}}} \end{aligned} \quad (3)$$

Here,  $pK_n$  is the acid dissociation constant associated with valence state  $n$ . Persat et al. [12] review the topic of effective mobility of weak and strong electrolytes including pH and ionic strength effects. In this work, we measure  $\mu_{i,\text{eff}}$  as a function of pH and for a range of ionic strengths and the use this to quantify actual mobilities ( $\mu_{i,z}$ ) and relevant acid dissociation constants ( $pK_n$ ), as per relations (2) and (3).

Ionic strength also influences the observable and actual mobilities of a species. Briefly, increasing ionic strength monotonically decreases (effective or actual) mobility, and the influence of ionic strength is stronger for higher valence values [13, 35]. We, therefore, correct our measurements for this effect to extract the estimates for the fully ionized mobility of an isolated ion (i.e. in the limit of negligibly small ionic strength). The latter ideal quantity has been termed the ion absolute mobility,  $\mu_{i,z}^0$ , which is the quantity of most interest. Given estimates of  $\mu_{i,z}^0$  and electrophoresis theory, we can predict a wide range of effective (observable) mobility values for wide ranges of pH and ionic strength.

Onsager and Fuoss [35] proposed a model of the ionic strength dependence of an ion’s absolute mobility for an arbitrary mixture of species. However, the Onsager–Fuoss model treats the ions as point charges, and this limits its applicability to ionic strengths equal to or lower than order 1 mM. The Onsager–Fuoss model can be extended to higher ionic strengths by, for example, including the finite ionic radius correction of Pitts et al. [36]. This extended Onsager–Fuoss model for ionic strength dependence of mobility of  $i$ th species in a mixture of  $s$

different species can be written as [13, 37]

$$\mu_i = \mu_i^0 - (A\mu_i^0 + B) \frac{\sqrt{\Gamma}}{1 + (aD/\sqrt{2})\sqrt{\Gamma}} \quad (4)$$

$$A = z_i \frac{e^3}{12\pi} \sqrt{\frac{N_{AV}}{\epsilon kT}} \sum_{n=0}^{\infty} C_n R_i^n, \quad B = |z_i| \frac{e^2}{6\pi\eta} \sqrt{\frac{N_{AV}}{\epsilon kT}}$$

$$D = \sqrt{\frac{2e^2 N_{AV}}{\epsilon kT}}, \quad \Gamma = \sum_{i=1}^s \Gamma_i, \quad \Gamma_i = c_i z_i^2$$

Here  $z_i$  is the charge number of the  $i$ -th ionic species,  $e$  the elementary charge,  $k$  the Boltzmann constant,  $N_{AV}$  the Avogadro constant,  $T$  the temperature, and  $\Gamma$  is twice the ionic strength  $I$  ( $0.5 \sum_i c_i z_i^2$ ). The coefficients  $C_n$  and the vectors  $\mathbf{R}^n = [R_1^n, R_2^n, \dots, R_s^n]^T$  are given in [35]. In Eq. (4),  $a$  represents the mean distance of the closest approach for the ions. For our calculations, we chose a fixed value  $1.5 \text{ mol}^{-1/2} \text{ m}^{3/2}$  for  $a$  [13].

We here measure the effective mobilities of fluorescent dyes for pH and ionic strengths ranging from 4 to 10 and 30 to 90 mM, respectively. We fit expressions (2) and (3) to the measured, effective mobilities for varying pH's to simultaneously determine the actual mobilities ( $\mu_{i,z}$ ) and relevant dissociation constants ( $pK_a$ ). We then correct the actual mobilities for finite ionic strength effects using the extended Onsager–Fuoss model, given by Eq. (4), to obtain the estimates of the absolute mobilities of ionic species (the ideal, fully ionized mobility at infinite dilution) corresponding to each relevant dissociation level of our fluorescent dyes.

We quantify the effective mobility of a species in a standard way, by applying an electric field and noting its migration time between a point of injection and a detector. The apparent mobility is calculated, given migration time and electric field, as

$$\mu_{i,\text{app}} = \frac{v_i}{E} = \frac{L}{Et_i} \quad (5)$$

where  $L$  is the length between the point of injection and detector,  $E$  the electric field,  $t_i$  the migration time and  $v_i = L/t_i$  the electrophoretic velocity of species  $i$ . As usual, we obtain the effective mobility from  $\mu_{\text{app},i}$  by accounting for EOF mobility,  $\mu_{\text{EOF}}$ . We quantify  $\mu_{\text{EOF}}$  by measuring the migration time  $t_{\text{EOF}}$  of a neutral species during the same experiment. The EOF mobility  $\mu_{\text{EOF}}$  is obtained given the electroosmotic velocity  $v_{\text{EOF}}$  by

$$\mu_{\text{EOF}} = \frac{v_{\text{EOF}}}{E} = \frac{L}{Et_{\text{EOF}}} \quad (6)$$

Combining these simple relations, we can write for the effective mobility

$$\mu_{i,\text{eff}} = \mu_{i,\text{app}} - \mu_{\text{EOF}} = \frac{L}{E} \left( \frac{1}{t_i} - \frac{1}{t_{\text{EOF}}} \right) \quad (7)$$

We used glass microchannels, where negative surface charge yields EOF in the direction of the electric field. Anions with electrophoretic mobility magnitudes lower than that of the EOF mobility, therefore, have net velocity directed towards the negative electrode (cathode). This allows for

having a single detector for both anions and cations on the cathode side.

Estimation of effective mobility using Eq. (7) requires accurate measurements of migration times  $t_i$ ,  $t_{\text{EOF}}$ ,  $E$ , and  $L$ . The chips we used have variable cross-sectional area channels (cf. Fig. 1), for which there are several choices in quantifying the local  $E$  in the separation channel section (which has locally uniform cross-section). For example, one method is to obtain precise estimates of local channel cross-sectional area  $A$ , applied current  $I$ , and the  $\sigma$  electrical conductivity of electrolyte solution to relate electric field as  $E = I/(\sigma A)$ . This requires current measurement of each individual run. Here, we chose to estimate  $E$  by using the analogy between electrokinetic chips of this type (for which electromigration current is dominant over diffusive and advection current components) and a simple resistor network. We provide details in the Supporting Information Section (see Fig. S1 and discussion). Briefly, our circuit model relates geometric channel parameters (channel lengths and cross-sectional area ratios) to compute the relationship between channel geometries, applied potentials, and electric fields. The latter method is independent of the value of electrolyte conductivity, and mapping system-wide electric fields also helps in optimizing injection

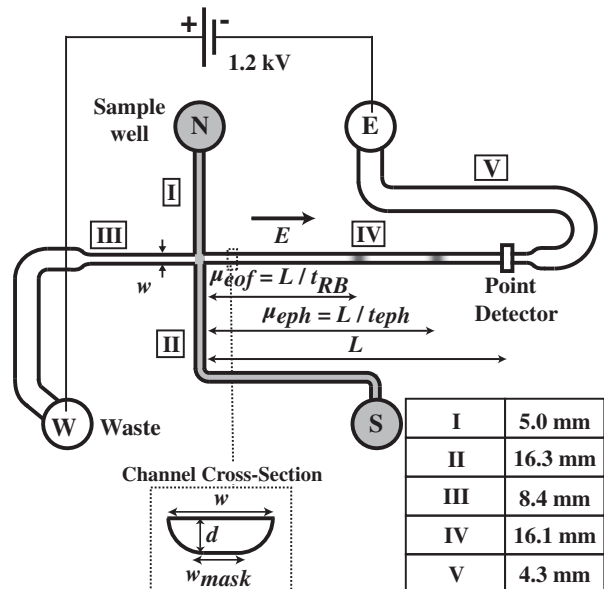


**Figure 1.** The experimental apparatus for CE includes microfluidic chip, epifluorescence microscope, CCD camera, high-voltage switching system, 1.2 kV DC power supply, and DAQ system. We used a  $10\times$  objective for all experiments. The exposure time varied between 50 and 100 ms depending on the signal strength. The chip used for all cases was a cross-type Caliper NS 95 with  $12 \mu\text{m}$  etch depth and  $10 \mu\text{m}$  mask width in the separation channel. Precise measurements of channel center contour lengths of various regions (e.g. region IV, the separation channel) are provided in the inset table. We used either one or two analytes and a neutral dye (RB) loaded into the north reservoir. The electric field along the separation channel was  $294 \text{ V/cm}$  oriented from left to right.

protocols. We also performed 2-D simulations (data not shown) of two-dimensional effects of electric fields (e.g. in channel turns) and concluded that such geometrical features have negligible effect on overall impedance (which is dominated by the channel curve centerline contour distances). Also, note that the molar concentration of our analyte fluorophores was in all cases  $\sim 3$  orders of magnitude less than that of our background buffers (so they contributed negligibly to channel impedance estimates).

## 3 Materials and methods

### 3.1 Chemicals and instrumentation

We performed controlled CE experiments in the pH range of 4.2–10.3 for determining effective mobility of FL, R6G, and AF488. We used anionic sodium FL (Molecular Probes, Eugene, OR, USA) at 300  $\mu\text{M}$ , anionic Alexa Fluor 488 succinimidyl ester at 150  $\mu\text{M}$  (Molecular Probes), and cationic R6G (Acros Organics, Geel, Belgium) at 150  $\mu\text{M}$ . R6G exists as two forms known, respectively, as dihydrorhodamine 6G and Rhodamine 6G chloride. Dihydrorhodamine 6G is uncharged and non-fluorescent. Dihydrorhodamine 6G oxidizes to become the charged Rhodamine 6G chloride which is fluorescent. We here studied Rhodamine 6G chloride. We used RB dye (Sigma-Aldrich, St. Louis, MO, USA) at 200  $\mu\text{M}$  to quantify EOF. RB has a reported  $\text{p}K_{\text{a}}$  value of 3.22 [38] and approximately neutral for our pH range of interest. We chose these dye concentrations to obtain electropherograms with comparable peak heights. We prepared buffer solutions of glycine, tricine, HEPES, MES, and acetic acid titrated with NaOH to pH's between 4.2 and 10.3. These 15 electrolyte chemistries are summarized in Table 1. We diluted all stock buffer solutions with deionized ultrafiltered water (DIUF) (Fischer Scientific, Pittsburgh, PA, USA). We used both PeakMaster [37] and SPRESSO [39] to aid in buffer design and analysis (both codes gave the same results). Predicted pH values often differed by  $\sim 0.1$ – $0.2$  pH units from measured values, possibly due to the effects of ionic strength [13]. Hence, we report both predicted and measured pH values for these buffers as determined using a Corning Pinnacle 542 pH/conductivity meter (Nova Analytics, Woburn, MA, USA). Lastly, we explored the effect of 0.1–2% by weight PVP (Polysciences, Warrington, PA, USA) on R6G mobility.

We performed all assays on a commercial NS-95 borosilicate microchip purchased from Caliper Life Sciences (Mountain View, CA, USA) with a simple cross-pattern consisting of narrow and wide channel sections, as shown in Fig. 1. The chip was wet etched and covered with a clear plate of the same material. Isotropically etched glass channels were 12  $\mu\text{m}$  in depth, and 11 and 50  $\mu\text{m}$  in mask width in the narrow and broad regions, respectively. The separation channel length was 16.1 mm.

We imaged the zones in the CZE experiment with an inverted epifluorescent microscope (IX70, Olympus,

Hauppauge, NY, USA) equipped with a mercury lamp, a U-MWIBA filter-cube from Olympus (460–490 nm excitation and 515 nm emission) and a  $10\times$  (NA of 0.4) UPlanApo objective for fluorescence imaging. Images were captured using a 12-bit, 1300 by 1030 pixel array CCD camera (Coolsnap, Roper Scientific, Trenton, NJ, USA), and with  $\mu$ -Manager microscopy software (available for free at [micro-manager.org](http://micro-manager.org)). We performed post-processing of the data with custom MATLAB scripts. High voltage was applied at microchip wells using a computer-controlled Labsmith HVS-3000D (Livermore, CA, USA) power supply and 10-mm lengths of 0.5 mm diameter platinum wire (Goodfellow, Oakdale, PA, USA) soldered to high-voltage leads.

### 3.2 Assay protocols

We empirically optimized the voltage scheme for sample injection. The scheme uses a fairly standard pinching and 'retraction' step and is described in detail in the Supporting Information.

The point of detection to measure elution time was typically placed 15 mm down the separation channel as shown in Fig. 1. The only exception was experiments where we strongly suppressed EOF, where signal-to-noise ratio requirements compelled us to move it to only 1.5 mm from the injection region. For each run, we used a pipette to dispense 40  $\mu\text{L}$  volumes of the dye concentrations described earlier into the sample reservoir (so we consumed 6–12 ng of fluorophore for each experiment). Between each run, we used a channel-cleaning procedure similar to that of Chambers et al. [10]. To this end, we flushed the channel with 40  $\mu\text{L}$  of 0.5 M NaOH for 10 min by applying vacuum to the well S in Fig. 1, followed by deionized water for 5 min, 100 mM HCl for 3 min, and deionized water again for 3 min. Between each run, we found that flushing several times with deionized water was approximately sufficient in refreshing the surface to its initial state (although we quantified EOF for each and every run).

## 4 Results and discussion

### 4.1 Estimation of absolute mobility in CE experiments

As mentioned in Section 2, we measured migration times of both electrophoretic and neutral dyes to quantify the effective mobility of species given apparent mobility, using Eq. (7). We then performed nonlinear regression best fits of expressions (2) and (3) to the measured effective mobility versus pH data to obtain actual mobility (fully ionized mobility at finite ionic strength) and  $\text{p}K_{\text{a}}$ 's. We then correct the actual mobilities for finite ionic strength effects to obtain the absolute mobilities of fluorescent species. The absolute mobility and the  $\text{p}K_{\text{a}}$  associated with each valence state can be interpreted as an estimated material property for the dye.

**Table 1.** Description of buffer solutions used to study pH effects.

	Measured, predicted pH	<i>C</i> (acid) (mM)	<i>C</i> (base) (mM)	<i>I</i> (mM)
		Glycine (+1, 39.5, 2.32), (−1, 37.4, 9.78)	NaOH	
1	10.3, 10.11	40	30	30
2	9.8, 9.64	60	30	30
3	9.4, 9.16	120	30	30
		Tricine (−1, 26.6, 8.5)	NaOH	
4	8.5, 8.49	40	30	30
5	8.0, 8.00	60	30	30
6	7.6, 7.53	120	30	30
		HEPES (−1, 21.8, 7.5)	NaOH	
7	8.3, 7.84	40	30	30
8	7.7, 7.36	60	30	30
9	7.2, 6.88	120	30	30
		MES (−1, 26.8, 6.13)	NaOH	
10	6.6, 6.43	40	30	30
11	6.1, 5.95	60	30	30
12	5.7, 5.48	120	30	30
		Acetic acid (−1, 42.4, 4.756)	NaOH	
13	5.2, 5.09	40	30	30
14	4.7, 4.62	60	30	30
15	4.2, 4.14	120	30	30

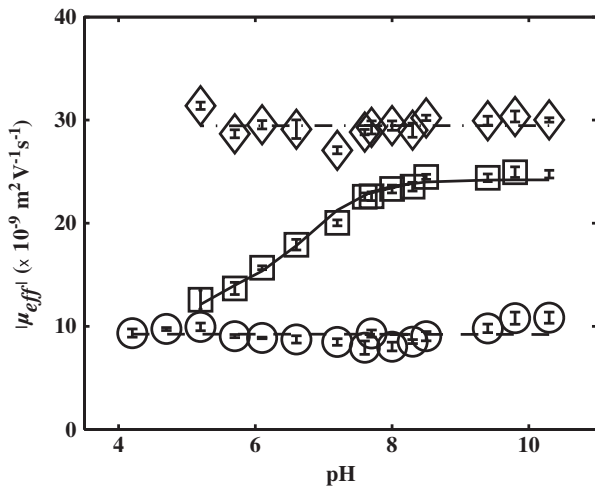
In parenthesis, we list, respectively, buffer valence, absolute mobility as  $10^{-9} \text{ m}^2/\text{V s}$  and  $\text{pK}_a$ .

Figure 2 shows the effective mobility measurements for FL, R6G, and AF488 versus pH at constant ion strength. Each data point is the mean of five realizations, and the error bars denote a 95% confidence interval based on Student *t*-distribution. As shown, the effective mobility of univalent cationic R6G and anionic AF488 is constant within the pH range of study. We know of no source reporting  $\text{pK}_a$ 's for R6G and AF488, and our experiments suggest that these fluorophores have no  $\text{pK}_a$  in the 3–10 pH range. However, the FL mobility initially increases with an increase in pH and subsequently plateaus at higher pH (~7–10). FL is a dibasic acid with a dissociation constant of the mono ion of ~6.8. Several groups report FL  $\text{pK}_a$ 's [38, 40] to be in the range of 2.1–2.2 (cation), 4.4 (neutral), and 6.7–6.8 (mono-anion). Due to its strong decrease in quantum yield at acid conditions [40, 41], we were unable to obtain data for FL below pH 5 (quantum yield of FL is maximum near pH 8). In contrast, R6G and AF488 exhibited approximately uniform fluorescence within the pH range 4–10. Similar behavior for AF488 was observed by Panchuk-Voloshina et al. [42].

Next, we determine the absolute mobilities and relevant  $\text{pK}_a$  of FL, R6G, and AF488 from the experimental data. We

summarize the values and relevant relations in Table 2. We numerically calculated the following absolute mobilities for R6G and AF488:  $-14 \times 10^{-9}$  and  $36 \times 10^{-9} \text{ m}^2/\text{V s}$ , corresponding to −1 and +1 valences, respectively. FL shows two absolute mobilities:  $19 \times 10^{-9}$  and  $36 \times 10^{-9} \text{ m}^2/\text{V s}$ , corresponding to −1 and −2 valence states. By comparison, the effective mobility value for FL has been reported as  $33.5 \pm 0.2 \times 10^{-9} \text{ m}^2/\text{V s}$  in 1 mM Tris-HCl solution at pH 9.1 [31]. This value is consistent with our experimental data and other reported data at similar conditions [29, 30]. Our effective mobility curves for R6G and AF488 (Eq. 2), and FL (Eq. 3) are shown in Fig. 2 along with the experimental data for 30 mM ionic strength. Khurana et al. [43] report a  $\text{pK}_a$  of 7.5 for the related species dihydrorhodamine 6G but not for the species Rhodamine 6G chloride of interest here; a value they obtained using an ARChem (Automated Reasoning in Chemistry) physicochemical property calculator SPARC (<http://sparc.chem.uga.edu/sparc>). Duvvuri et al. [44] reported an experimental value of 7.5 for dihydrorhodamine 6G as well. Another group [45] found (experimentally) that the alkalinity of a Rhodamine 6G species (the molecular structure was not specified) varied with light excitation and reported a  $\text{pK}_a$  value of 6.5. We know of no other reported values.

In Table 2, we also report diffusivities as per Nernst–Einstein relation ( $D_i = RT\mu_{i,\text{eff}}$ ), where we use the absolute mobility values (at infinite dilution). We calculated the



**Figure 2.** Effective mobility data for Rhodamine 6G, Fluorescein, and Alexa Fluor 488 at 30 mM ionic strength and pH between ~4.2 and 10.4. Shown are experimental data for R6G (○), fluorescein (□), and AF488 (◇). We show fits for effective mobility of R6G (---), fluorescein (—), and AF488 (---) 30 mM ionic strength. Fluorescein displays a  $pK_a$  at pH ~7. R6G and AF 488 seem to be fully ionized within the range. We performed a total of five repetitions for each case and show here the mean value. The error bars correspond to 95% confidence intervals on the means with  $N=5$  realizations at each pH. The least-squares curve fit the data using effective mobility theory, including correcting for ionic strength based on an Onsager and Fuoss model with a Pitts correction [13]. For this theory, we assumed two  $pK_a$  values (4.45 and 6.8) reported in literature for FL, and use the fit to extract effective mobility data. FL has a third  $pK_a$  (2.14), but this falls well outside the pH range of the experiments. From these data, we calculated the absolute mobility values of  $19 \times 10^{-9}$  and  $36 \times 10^{-9} \text{ m}^2/\text{V s}$ , corresponding to  $-1$  and  $-2$  valence states for fluorescein. We did not observe  $pK_a$ 's for AF 488 and R6G within this pH range. Their pH-averaged, absolute mobilities are  $36 \times 10^{-9}$  and  $14 \times 10^{-9} \text{ m}^2/\text{V s}$ , respectively.

diffusivities for FL, AF488, and R6G as  $9.3 \times 10^{-10}$ ,  $9.3 \times 10^{-10}$ , and  $3.6 \times 10^{-10} \text{ m}^2/\text{s}$ , respectively. Magde et al. [46] used fluorescence correlation spectroscopy (FCS) and reported  $D_{R6G} = 2.80 \text{ m}^2/\text{s}$  at  $22^\circ\text{C}$ . Petrasek and Schwillie [47] reported measured values of  $D_{R6G} = 4.26 \text{ m}^2/\text{s}$  at  $22.5^\circ\text{C}$  using FCS. Muller et al. [48] reported a value of  $D_{R6G} = 4.14 \text{ m}^2/\text{s}$  at  $25^\circ\text{C}$  using multicolor dual focus FCS. Corrected for temperature effects (absolute viscosity and absolute temperature on diffusivity as per Einstein relation), these reported values are within about 14 and 8% of our measured value, respectively.

We note that the ambient temperature for our experiments varied between 21 and  $23^\circ\text{C}$ ; however, we consider a more conservative range of a  $3^\circ\text{C}$  variation. We estimate the maximum variations in mobility from the expected variation in dynamic viscosity of water for our aqueous solutions. A  $\pm 1.5^\circ\text{C}$  variation in temperature results in about  $\pm 3\%$  of absolute viscosity (using the viscosity versus temperature fit reported by Touloukian et al. [49]). Therefore, the absolute values of mobilities presented here varied with temperature by as much as  $\pm 2.4\%$  for R6G and  $\pm 1.0\%$  for FL and AF488. These estimated variations can be compared with the observed experimental uncertainties from the mean for five realizations (using 95% confidence interval and the Student  $t$ -distribution). The latter uncertainties were 3.9% (R6G), 1.9% (FL), and 1.5% (AF488).

As a further comparison, we also report a second set of absolute mobility estimates based on a reference effective mobility value of  $33.5 \pm 0.2 \times 10^{-9} \text{ m}^2/\text{V s}$  for FL at  $27^\circ\text{C}$ , pH 9.1 (from [31]). In these additional mobility estimates, we first extrapolate this published FL value to  $22^\circ\text{C}$  using Walden's rule [34] and the aforementioned viscosity versus temperature fit by Touloukian et al. [49]. The extrapolation yields a new reference value of  $32.4 \pm 0.2 \times 10^{-9} \text{ m}^2/\text{V s}$  for FL at  $22^\circ\text{C}$ . We then assume that this reference effective mobility at  $22^\circ\text{C}$  is correct and use it to normalize all of our effective mobility data for AF488 and R6G. To this end, we use the FL reference value to obtain new electric field estimates, construct mobility

**Table 2.** Absolute mobilities (i.e. fully ionized value extrapolated to 0 ionic strength) and diffusivities based on these absolute mobility estimates (as per Nernst–Einstein diffusion) for fluorescein, R6G, and AF488 (at  $22^\circ\text{C}$ ), their  $pK_a$ 's and prediction models

Fluorophore	$\mu_{\text{abs, expt.}, 22^\circ\text{C}}$ $\mu_{\text{abs, ref.}, 22^\circ\text{C}}$ ( $\times 10^{-9} \text{ m}^2/\text{V s}$ )	$pK_a$ 's	Relation for $\mu_{\text{eff}}$ ( $\times 10^{-9} \text{ m}^2/\text{V s}$ )	$D$ ( $\times 10^{-10} \text{ m}^2/\text{s}$ )
Fluorescein	35.9 34.5	4.4 6.8	$\mu_{i,\text{eff}} = \frac{\mu_{i,-1}^0 + \mu_{i,-2}^0 10^{\text{pH}_i - \text{p}K_{i,-2}}}{1 + 10^{\text{p}K_{i,-1} - \text{pH}_i} + 10^{\text{pH}_i - \text{p}K_{i,-2}}}$	9.3
Alexa Fluor 488	36.0 36.1	— <sup>a)</sup>	$\mu_{i,\text{eff}} = \mu_{i,-1}^0 \frac{1}{1 + 10^{\text{p}K_{i,-1} - \text{pH}_i}} \cong \mu_{i,-1}^0$	9.3
Rhodamine 6G	14.0 12.6	— <sup>a)</sup>	$\mu_{i,\text{eff}} = \mu_{i,+1}^0 \frac{1}{1 + 10^{\text{pH}_i - \text{p}K_{i,+1}}} \cong \mu_{i,+1}^0$	3.6

We report two absolute mobility values: our experimental values and values assuming a reference FL effective mobility [31] extrapolated to  $22^\circ\text{C}$ .

a)  $pK_a$ 's for Rhodamine 6G chloride and Alexa Fluor 488 are well outside the pH range used in these experiments. We know of no reported values in literature.

curves, and calculate the respective new absolute mobilities for FL, AF488, and R6G. In Table 2, we include these ‘normalized’ absolute mobility estimates for FL, AF, and R6G at 22°C (the second value in each row of the mobility column). The absolute mobility values obtained directly from the experimental data agree well with mobilities normalized to this reference value.

We note we explored the possible effect of Joule heating on our measured mobilities. For all of the chemistries explored, we verified that Joule heating was insignificant by monitoring current versus voltage traces. The current versus applied voltage data was clearly linear over as much as twice the maximum voltages used in our experiments. This linearity implies negligible effects of Joule heating. In the Supporting Information document, we include a figure (Fig. S2) of the current versus voltage trace for the highest conductivity buffer (90 mM NaOH, 180 mM Glycine) and applied voltages ranging from 250 to 2000 V (which yielded a linear relation with a regression coefficient of  $R = 0.997$ ).

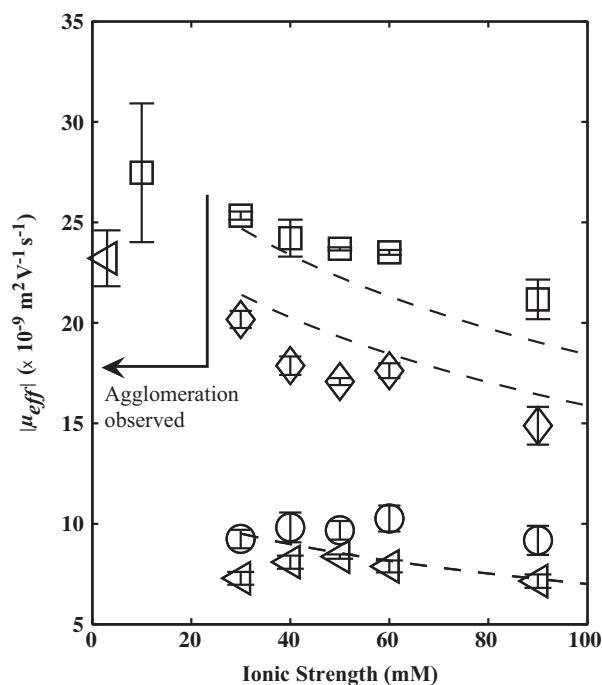


**Figure 3.** Effective mobility data for R6G at pH 7.2 ( $\blacktriangle$ ), R6G at pH 9.4 ( $\circ$ ), FL at pH 7.2 ( $\diamond$ ), and FL at pH 9.4 ( $\square$ ) and numerical predictions (---). We based the numerical simulations leveraging the Onsager and Fuoss model and Spresso [35, 39]. The effective mobility for R6G approximately levels off at higher concentrations (>30 mM) and decreases only slightly with decreasing pH. (Below, we discuss R6G adsorption–desorption behavior and how this may affect the results.) Fluorescein mobility decreases more drastically with ionic strength increase. FL mobility at pH 7.2 is lower than at pH 9.4, irrespective of ionic strength, consistent with the results in Fig. 2. The data below ~20 mM for both R6G and FL are not representative of mobility data as we observed precipitation of the neutral marker RB in that regime. This precipitation impeded our ability to quantify EOF.

## 4.2 Effect of ionic strength

In Fig. 3, we show measurements of effective mobilities for FL and R6G at pH 9.4 and 7.2 (each) and eight ionic strengths in a range between 3 and 90 mM. FL is a divalent acid while R6G is monovalent, so the stronger dependence of FL to ionic strength is expected. FL mobility drops ~20–25% (depending on the pH) as ionic strength increases from 30 to 90 mM. On the other hand, R6G shows only weak dependence on ionic strength. Predictions based on extended Onsager and Fuoss model [13, 37] are shown as dashed curves, and these show fairly good agreement with our experimental data. We attempted but were unable to obtain accurate, meaningful data below ionic strengths of 30 mM. After a series of control experiments, we concluded that RB precipitates and forms observable aggregates below about 20 mM. Our observations suggest that RB interacts strongly with the channel walls in this regime, strongly impeding (and biasing) our efforts to quantify EOF mobility. Such a behavior has been reported for RB [50, 51].

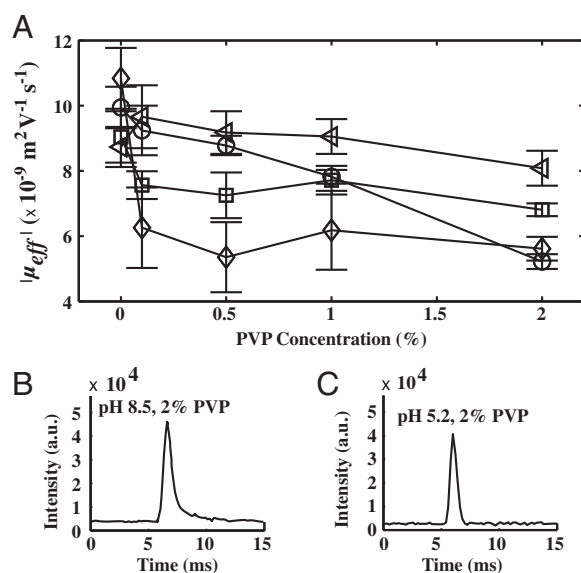


**Figure 4.** (A) Effective mobility of R6G at 0, 0.1, 0.5, 1, and 2% polyvinylpyrrolidone (PVP) for: pH 5.2 ( $\circ$ ), 6.6 ( $\triangle$ ), pH 8.5 ( $\square$ ), and 10.3 ( $\diamond$ ). We show the example electropherograms for R6G at pH 8.5 (B) and pH 5.2 (C) each with PVP concentration of 2%. These R6G mobility data correct for EOF using RB elution time measurements. The addition of PVP polymer decreased EOF significantly, so we placed the detection point 1.5 mm downstream of the channel intersection for enhanced signal-to-noise ratio. R6G shows no  $pK_a$  within the working range, so we hypothesize that its mobility varies with pH due to its interactions with the channel walls. The data with highest reproducibility were for pH of 5.2 and 6.6 data and high PVP concentration (1 and 2%). These cases exhibit no peak tailing which we attributed to adsorption/desorption phenomena. Electropherograms (B and C) show peak tailing at pH 8.5 with 2% PVP but no tailing for the same PVP concentration and pH 5.2.

### 4.3 Effects of PVP on mobility

We also measured the effective mobilities of FL, R6G, and AF488 in the presence of the dynamic-coating PVP polymer. We explored PVP concentrations from 0 to 2% and pH values of 5.2, 6.6, 8.5, and 10.3 with a fixed ionic strength of 30 mM. We found that PVP changed the mobilities of FL and AF488 by amounts less than about our experimental uncertainty (approximately  $\pm 1 \times 10^{-9} \text{ m}^2/\text{Vs}$ ) through this PVP and pH range, and so these will not be discussed further here. However, PVP had a strong influence on the measurements of R6G mobilities. R6G is a cationic dye and as such more susceptible to wall interactions in our borosilicate glass channels. Figure 4 presents the measurements of the effective mobility of R6G. As with the data discussed earlier, we used measurements of RB elution times to correct for the strong effects of EOF suppression by PVP. (We will present a study of the effects of PVP suppression of EOF in a future publication.) The data of Fig. 4 show that R6G effective mobility mostly decreases with increasing PVP concentration. At and above pH 6.6, we see a monotonic decrease of mobility with increasing pH. The pH 5.2 data have the most pronounced decrease with decreasing PVP concentration. We hypothesize that R6G mobility varies due to interactions with channel walls. Analysis of the individual R6G peak shapes supports this hypothesis. Notably, high pH for both low and high PVP concentrations results in noticeable tailing of R6G peaks, suggesting wall adsorption/desorption-type dynamics [52]. We show Fig. 4B and C as typical example data showing pronounced tailing for pH 8.5 but not pH 5.2. We note that Hamai and Sasaki [53] also reported dispersion of R6G peaks due to polyvinyl sulfate (PVS). Their data and discussion suggest that this is due to direct interactions between R6G and PVS. We did not observe such interactions. Instead, our observations show significant tailing of R6G peaks in the absence of PVS.

### 5 Concluding remarks

We have presented experimental data of absolute and effective electrophoretic mobilities and diffusivity estimates for FL, R6G, and AF488. We performed on-chip CE experiments for various pH's, ionic concentrations, and concentrations of the EOF-suppressing polymer PVP. We used RB as a neutral fluorescent marker to account for EOF in each experiment. Experimentally, we observed that the mobility curve is nearly horizontal for both R6G and AF488, and has a sigmoid-like shape for FL. This behavior is consistent with a  $pK_a$  of  $\sim 6.8$  for FL (within this pH range) and the absence of a  $pK_a$  in this range for both R6G and AF488. We accounted for and corrected for the influence of ionic strength on sample analytes. We demonstrated that analyte mobility decreases with increasing ionic strength. This effect is more pronounced for the divalent FL than for univalent R6G, as predicted by Onsager and Fuoss theory as extended by Pitts. Based on

experimental data, we concluded that ionic strength should be at least 20 mM to prevent aggregation of the neutral marker RB. We pointed out that reduced adsorption is critical for clean and accurate separation. We further studied the effect of the EOF suppressant PVP on the mobilities of FL, AF488, and R6G. We found a negligible effect of PVP on FL and AF488. However, we found a strong PVP effect on R6G mobility, which we attribute to adsorption–desorption dynamics of the cationic R6G dye with our negatively charged channel walls. We found an addition of 2% PVP at low pH ( $\sim 5.2$ ) reduces EOF more than  $100\times$  and R6G is well behaved. Adsorption–desorption of R6G is apparently very important at high pH, as evidenced by mobility trends and pronounced tailing of the signal peaks. Overall, on-chip CZE offers fairly rapid, highly reproducible mobility measurements that require very little sample use.

*The authors have declared no conflict of interest.*

### 6 References

- [1] Gryczynski, Z., Gryczynski, I., Lakowicz, J. R., *Biophotonics*, Pt A, Academic Press, Inc., San Diego 2003, pp. 44–75.
- [2] Kricka, L. J., Fortina, P., *Clin. Chem.* 2009, *55*, 670–683.
- [3] Sameiro, M., Goncalves, T., *Chem. Rev.* 2009, *109*, 190–212.
- [4] Opitz, N., Lubbers, D. W., *Sens. Actuators* 1983, *4*, 473–479.
- [5] Shimura, K., *Electrophoresis* 2009, *30*, 11–28.
- [6] Slais, K., Horka, M., Novackova, J., Friedl, Z., *Electrophoresis* 2002, *23*, 1682–1688.
- [7] Lacroix, M., Poinsot, V., Fournier, C., Couderc, F., *Electrophoresis* 2005, *26*, 2608–2621.
- [8] Moser, A. C., Hage, D. S., *Electrophoresis* 2008, *29*, 3279–3295.
- [9] Bercovici, M., Kaigala, G. V., Backhouse, C. J., Santiago, J. G., *Anal. Chem.* 2010, *82*, 1858–1866.
- [10] Chambers, R. D., Santiago, J. G., *Anal. Chem.* 2009, *81*, 3022–3028.
- [11] Probstein, R. F., *Physicochemical Hydrodynamics: An Introduction*, John Wiley & Sons, Inc., New York 1994.
- [12] Persat, A., Suss, M. E., Santiago, J. G., *Lab Chip* 2009, *9*, 2454–2469.
- [13] Bahga, S., Bercovici, M., Santiago, J. G., *Electrophoresis* 2010, *31*, 910–919.
- [14] Barron, D., Jimenez-Lozano, E., Barbosa, J., *J. Chromatogr. A* 2001, *919*, 395–406.
- [15] Beckers, J. L., Everaerts, F. M., Ackermans, M. T., *J. Chromatogr.* 1991, *537*, 407–428.
- [16] Canals, I., Bosch, E., Roses, M., *Anal. Chim. Acta* 2002, *458*, 355–366.
- [17] Porras, S. P., Riekkola, M. L., Kenndler, E., *J. Chromatogr. A* 2001, *905*, 259–268.

- [18] Vcelakova, K., Zuskova, I., Kenndler, E., Gas, B., *Electrophoresis* 2004, 25, 309–317.
- [19] Zuskova, I., Novotna, A., Vcelakova, K., Gas, B., *J. Chromatogr. B* 2006, 841, 129–134.
- [20] Williams, B. A., Vigh, C., *Anal. Chem.* 1996, 68, 1174–1180.
- [21] Hirokawa, T., Gojo, T., Kiso, Y., *J. Chromatogr.* 1986, 369, 59–81.
- [22] Hirokawa, T., Nishino, M., Kiso, Y., *J. Chromatogr.* 1982, 252, 49–65.
- [23] Pospichal, J., Deml, M., Bocek, P., *J. Chromatogr.* 1987, 390, 17–26.
- [24] Pospichal, J., Deml, M., Zemlova, Z., Bocek, P., *J. Chromatogr.* 1985, 320, 139–146.
- [25] Andersson, E. K. M., *J. Chromatogr. A* 1999, 846, 245–253.
- [26] Urbanek, M., Varenne, A., Gebauer, P., Krivankova, L., Gareil, P., *Electrophoresis* 2006, 27, 4859–4871.
- [27] Garcia-Schwarz, G., Bercovici, M., Marshal, L., Santiago, J. G., *J. Fluid Mechanics* 2011, 679, 455–475.
- [28] Schonfeld, F., Goet, G., Baier, T., Hardt, S., *Phys. Fluids* 2009, 21, 092002-1-11.
- [29] Paul, P. H., Garguilo, M. G., Rakestraw, D. J., *Anal. Chem.* 1998, 70, 2459–2467.
- [30] Shakalisava, Y., Poitevin, M., Viovy, J. L., Descroix, S., *J. Chromatogr. A* 2009, 1216, 1030–1033.
- [31] Whang, C. W., Yeung, E. S., *Anal. Chem.* 1992, 64, 502–506.
- [32] Kaniansky, D., Masar, M., Bielikova, J., *J. Chromatogr. A* 1997, 792, 483–494.
- [33] Schutzner, W., Fanali, S., Rizzi, A., Kenndler, E., *J. Chromatogr. A* 1996, 719, 411–420.
- [34] Porras, S. P., Riekkola, M. L., Kenndler, E., *Electrophoresis* 2003, 24, 1485–1498.
- [35] Onsager, L., Fuoss, R. M., *J. Phys. Chem.* 1932, 36, 2689–2778.
- [36] Pitts, E., Tabor, B. E., Daly, J., *Trans. Faraday Soc.* 1970, 66, 693.
- [37] Jaros, M., Vcelakova, K., Zuskova, I., Gas, B., *Electrophoresis* 2002, 23, 2667–2677.
- [38] McHedlovpetrossyan, N. O., Kukhtik, V. I., Alekseeva, V. I., *Dyes Pigment* 1994, 24, 11–35.
- [39] Bercovici, M., Lele, S. K., Santiago, J. G., *J. Chromatogr. A* 2009, 1216, 1008–1018.
- [40] Martin, M. M., Lindqvist, L., *J. Lumines.* 1975, 10, 381–390.
- [41] Diehl, H., Markuszewski, R., *Talanta* 1989, 36, 416–418.
- [42] Panchuk-Voloshina, N., Haugland, R. P., Bishop-Stewart, J., Bhalgat, M. K., Millared, P. J., Mao, F., Leung, W. Y., *J. Histochem. Cytochem.* 1999, 47, 1179–1188.
- [43] Khurana, T. K., Santiago, J. G., *Lab Chip* 2009, 9, 1377–1384.
- [44] Duvvuri, M., Gong, Y. P., Chatterji, D., Krise, J. P., *J. Biol. Chem.* 2004, 279, 32367–32372.
- [45] Kuznetsov, R. T., Fofonova, R. M., *J. Appl. Spectrosc.* 1984, 40, 380–384.
- [46] Magde, D., Elson, E. L., Webb, W. W., *Biopolymers* 1974, 13, 29–61.
- [47] Petrasek, Z., Schwille, P., *Biophys. J.* 2008, 94, 1437–1448.
- [48] Muller, C. B., Loman, A., Pacheco, V., Koberling, F., Willbold, D., Richterig, W., Enderlein, J., *EPL* 2008, 83, 5.
- [49] Touloukian, Y. S., Saxena, S.C., Hestermans, P., *Thermophysical Properties of Matter*, The TPRC Data Series, Plenum Publishing Corp., New York 1975.
- [50] Ilich, P., Mishra, P. K., Macura, S., Burghardt, T. P., *Spectrosc. Acta Pt. A Mol. Biomol. pectrosc.* 1996, 52, 1323–1330.
- [51] McHedlov-Petrosyan, N. O., Kholin, Y. V., *Russ. J. Appl. Chem.* 2004, 77, 414–422.
- [52] Shariff, K., Ghosal, S., *Anal. Chim. Acta* 2004, 507, 87–93.
- [53] Hamai, S., Sasaki, K., *Microchem. J.* 2001, 69, 27–36.
- [54] Bharadwaj, R., Santiago, J. G., Mohammadi, B., *Electrophoresis* 2002, 23, 2729–2744.